The Rician Complex Envelope under Line of Sight Shadowing

Browning, J. W., Cotton, S. L., Morales-Jimenez, D., & Lopez-Martinez, F. J. (2019). The Rician Complex Envelope under Line of Sight Shadowing. *IEEE Communications Letters*, *23*(12), 2182-2186. https://doi.org/10.1109/LCOMM.2019.2939304

Published in:
IEEE Communications Letters

Document Version:
Peer reviewed version

The Rician Complex Envelope under Line of Sight Shadowing

Jonathan W. Browning, *Student Member, IEEE,* Simon L. Cotton, *Senior Member, IEEE,*
David Morales-Jimenez, *Member, IEEE* and F. Javier Lopez-Martinez, *Senior Member, IEEE*

***Abstract*—This paper investigates a Rician complex envelope which is subject to line-of-sight (LOS) shadowing. In particular, exact closed-form expressions are obtained for the joint envelope-phase distribution, the distribution of the phase, and that of the quadrature and in-phase signal components. Using the new formulation for the phase distribution, we find that for increasing shadowing severity, the phase becomes progressively more disperse. Interestingly, the phase is shown to be unimodal. This illustrates that the relationship which is known to exist between the envelope of Rician fading which undergoes LOS shadowing and Hoyt fading does not extend to the phase. We also provide two applications of our new results which investigate the average bit error probability and the average symbol error probability for phase-based modulation schemes operating in LOS shadowed fading channels. The results are shown to provide excellent agreement with Monte Carlo simulations.**

***Index Terms*—Envelope-phase distribution, phase distribution, shadowed fading.**

I. Introduction

RICIAN fading is one of the most important and well understood signal propagation mechanisms in the literature. Its complex signal envelope is modeled by the combination of a dominant or line-of-sight (LOS) component and a single cluster of scattered waves. Under certain propagation conditions the LOS component can fluctuate due to shadowing, which is induced by obstacles in the local environment. This phenomenon has been studied in the context of land mobile satellite channels [1], underwater acoustic channels [2] and device-to-device communications under human body shadowing [3]. Notably, a range of first order statistics relating to its shadowed signal envelope have been derived e.g. the probability density function (PDF) [1] and cumulative distribution function (CDF) [4]. While these expressions are useful for developing many communications performance measures of interest, unfortunately they do not account for the phase properties of signals which undergo Rician fading with LOS shadowing.

At present, little is known about the phase of Rician fading channels which are subjected to LOS shadowing. Understanding the properties of the phase distribution is essential for the design of wireless systems. For example, when information is transmitted in the phase of a carrier, it can be used to determine the probability of error for *M*-phase signaling over fading channels using diversity [5]. Characterizing the phase is critical in the optimal design and synchronization of coherent receivers [6] and in the detection of *M*-ary phase-shift keying (PSK) signal constellations [7]. While the phase distributions for Rician [8], Nakagami-*m* [9], and η-μ [10] fading models have previously been investigated, such distribution remains unfortunately unknown when the Rician complex signal undergoes LOS shadowing.

In this letter, we derive a new closed-form expression for the phase distribution of Rician-faded signals undergoing LOS shadowing. This provides insights into how LOS shadowing affects the phase of the received signal, a question of practical relevance which has not been previously addressed in the literature. To obtain an analytical expression for the phase distribution, we derive the distributions of the quadrature and in-phase signal components, and the joint envelope-phase distribution, providing novel closed-form formulations of independent interest. Particularly noteworthy is the joint envelope-phase distribution: although results are available for Nakagami-*m* [9], η-μ [10], κ-μ [11], no studies or results are so far available for any LOS shadowed fading models. Subsequently, our results are applied to investigate the average bit error probability and the average symbol error probability of phase-based modulation techniques used in systems which are susceptible to LOS shadowed fading.

II. Complex Signal Model

Let $S = R\exp(j\Theta)$ represent the complex signal envelope, where R is the received signal envelope and Θ is the phase. Letting X and Y represent the in-phase and quadrature components respectively, it follows that, $S = X + jY$, $R^2 = X^2 + Y^2$, $\Theta = \arg(X + jY)$, $X = R\cos(\Theta)$ and $Y = R\sin(\Theta)$. Rician fading undergoing LOS shadowing has previously been modeled with the amplitude of the LOS component randomly fluctuating, following a Nakagami-m distribution [1]. Here we adopt a definition of the complex signal envelope where the LOS component is shaped by a Nakagami-m random variable [12], ξ, with m as the shape parameter and $\mathbb{E}[\xi^2] = 1$, where $\mathbb{E}[\cdot]$ is the expectation operator. This random variable simultaneously impacts both the in-phase and quadrature components, producing a random LOS fluctuation. The received signal power can be modeled as

The work of F. J. Lopez-Martinez was supported by the Spanish Government (Ministerio de Economia y Competitividad) and FEDER under grant TEC2017-87913-R.

J. W. Browning, S. L. Cotton and D. Morales-Jimenez are with the Centre for Wireless Innovation, ECIT Institute, Queen's University Belfast, Belfast BT3 9DT, U.K. (e-mail: jbrowning01@qub.ac.uk; simon.cotton@qub.ac.uk; d.morales@qub.ac.uk).

F. J. Lopez-Martinez is with the Departmento de Ingenieria de Comunicaciones, Universidad de Málaga, 29071 Málaga, Spain. (e-mail: fjlopezm@ic.uma.es).

$$f_Z(z) = \frac{2^{1-2m}\Gamma(2m)\sqrt{1+K}m^m\hat{r}^{2m-1}}{\Gamma(m)[\lambda^2(1+K)+m\hat{r}^2]^m}\exp\left(-\frac{z^2}{\hat{r}^2}(1+K)\right)\left[\frac{1}{\Gamma(\frac{1}{2}+m)}{}_1F_1\left(m;\frac{1}{2};\frac{(\lambda z)^2(1+K)^2}{\hat{r}^2(\lambda^2(1+K)+m\hat{r}^2)}\right)\right.$$
$$\left.+\frac{2\lambda z(1+K)}{\Gamma(m)\hat{r}\sqrt{\lambda^2(1+K)+m\hat{r}^2}}{}_1F_1\left(m+\frac{1}{2};\frac{3}{2};\frac{(\lambda z)^2(1+K)^2}{\hat{r}^2(\lambda^2(1+K)+m\hat{r}^2)}\right)\right] \quad (4)$$

$$f_{R,\Theta}(r,\theta) = \frac{rm^m(1+K)}{\pi\hat{r}^2(m+K)^{m+1/2}\Gamma(m)}\exp\left(-\frac{r^2(1+K)}{\hat{r}^2}\right)\left[\sqrt{K+m}\Gamma(m){}_1F_1\left(m;\frac{1}{2};\frac{r^2(1+K)}{\hat{r}^2}\Delta(\theta,\phi)\right)\right.$$
$$\left.+\left(\frac{r}{\hat{r}}\right)2\sqrt{K(1+K)}\cos(\theta-\phi)\Gamma\left(m+\frac{1}{2}\right){}_1F_1\left(m+\frac{1}{2};\frac{3}{2};\frac{r^2(1+K)}{\hat{r}^2}\Delta(\theta,\phi)\right)\right] \quad (5)$$

$$R^2 = (X_I+\xi p)^2 + (Y_Q+\xi q)^2, \quad (1)$$

where X_I and Y_Q are mutually independent Gaussian random processes with $\mathbb{E}[X_I] = \mathbb{E}[Y_Q] = 0$, $\mathbb{E}[X_I^2] = \mathbb{E}[Y_Q^2] = \sigma^2$, p and q are real numbers, which model the power of the LOS component.

The PDF of the envelope *R*, can be obtained from [12] by letting $\mu = 1$ (the number of multipath clusters) which gives

$$f_R(r) = \frac{2rm^m(1+K)}{\hat{r}^2(K+m)^m}\exp\left(-\frac{r^2(1+K)}{\hat{r}^2}\right) \times {}_1F_1\left(m;1;\frac{K(1+K)}{(K+m)}\frac{r^2}{\hat{r}^2}\right), \quad (2)$$

where ${}_1F_1(\cdot;\cdot;\cdot)$ is the Kummer confluent hypergeometric function [13, eq. 13.1.2] and $\hat{r}^2 = \mathbb{E}[R^2]$. The severity of the shadowing shaping the LOS component is characterized by m, the Nakagami-m shape parameter; shadowing of the LOS component increases as $m \to 0$, while such shadowing vanishes as $m \to \infty$. The Rician K factor represents the ratio between the total power of the LOS component d^2, with $d^2 = p^2+q^2$, and the total power of the scattered components $2\sigma^2$, that is, $K = \frac{p^2+q^2}{2\sigma^2}$,where $2\sigma^2 = \frac{\hat{r}^2}{(1+K)}$. By defining $\phi = arg(p+jq)$ as a phase parameter, $p = \sqrt{\frac{K}{1+K}}\hat{r}\cos(\phi)$ and $q = \sqrt{\frac{K}{1+K}}\hat{r}\sin(\phi)$.

III. PDFs of In-Phase & Quadrature Components

We begin by letting $Z = X$ or $Z = Y$ and $\lambda = p$ or $\lambda = q$ as required to represent either the in-phase or quadrature components of the received signal. The model presented in (1) implies that when Z is conditioned on ξ, it follows a Gaussian distribution [7, eq. 2.3-8] (substituting $2\sigma^2$) given by

$$f_{Z|\xi}(z;\xi) = \frac{\sqrt{1+K}}{\sqrt{\pi}\,\hat{r}}\exp\left(-\frac{(z-\xi\lambda)^2}{\hat{r}^2}(1+K)\right). \quad (3)$$

From (3), the PDF of the in-phase and quadrature components can be obtained by averaging over ξ. The result is given below.

Theorem 1. *For $K, m, \hat{r}, \lambda \in \mathbb{R}^+, z \in \mathbb{R}$ the PDF of the in-phase ($Z = X, \lambda = p$) or quadrature ($Z = Y, \lambda = q$) component is given by (4), where $\Gamma(\cdot)$ is the Gamma function.*

Proof: See Appendix A. ■

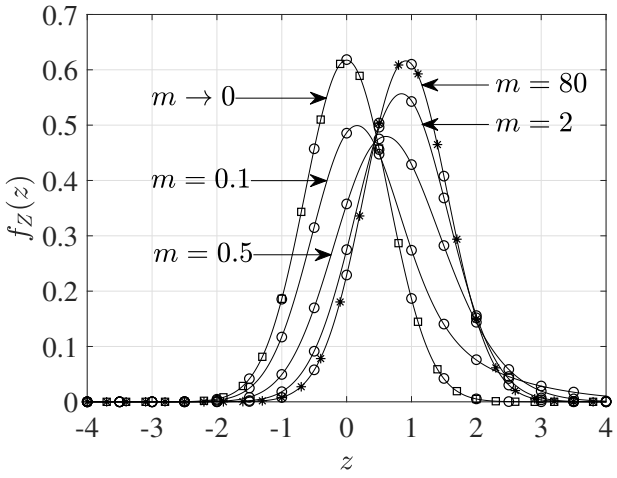

Fig. 1. Quadrature PDF given in (4) (solid lines) alongside Monte Carlo simulation (circles) for $K = 2, \hat{r}^2 = 2.5$, $m \to 0$ and $m = 0.1, 0.5, 2, 80$. For comparison, the Gaussian quadrature PDFs of the corresponding Rayleigh (squares) and Rician (asterisks) fading are also included.

To validate the accuracy of our new expressions, comparisons with some complementary Monte Carlo simulations are also included in the figures. In our simulations, we form (1) using 10^7 realizations of X_I, Y_Q and ξ. In Fig. 1 it can be seen when $m \to 0$ (i.e. the LOS component vanishes) that the shape of the resulting PDF becomes more Gaussian-like with zero mean, corresponding to the Rayleigh case. As $m \to \infty$ (i.e. the LOS component is not affected by shadowing), it reduces to a Gaussian distribution with mean $\lambda = q$, corresponding to Rician fading when there is no shadowing of the LOS component.

IV. Joint envelope-phase PDF

We now derive the joint distribution of the envelope and phase. Aside from being instrumental to the study of the phase, the following result has independent value, as it may be used to determine higher order statistics for single or multi-branch diversity systems [14].

Theorem 2. *For $K, m, \hat{r}, r \in \mathbb{R}^+, \phi, \theta \in [-\pi, \pi)$ the joint envelope-phase PDF is given by (5) with*

$$\Delta(\theta,\phi) = \frac{K\cos^2(\theta-\phi)}{(K+m)}. \quad (6)$$

$$f_\Theta(\theta) = \frac{m^m}{2\sqrt{\pi}(K+m)^{m+1/2}}\left[\sqrt{\frac{K+m}{\pi}}\,{}_2F_1\left(m,1;\frac{1}{2};\Delta(\theta,\phi)\right) + \frac{\Gamma\left(\frac{1}{2}+m\right)\sqrt{K}}{\Gamma(m)}\cos(\theta-\phi)\big(1-\Delta(\theta,\phi)\big)^{-m-1/2}\right] \quad (8)$$

Proof: See Appendix B. ■

An immediate corollary of Theorem 2 is that the envelope and phase are not independent, as can be observed from the joint PDF (5). Let us now explore some special cases. Letting $m \to \infty$ in (5) and using the fact that ${}_1F_1\big(a;b;0\big) = 1$ [15] results in the Rician joint envelope-phase PDF [8],

$$f_{R,\Theta}(r,\theta) = \frac{r(1+K)}{\pi\hat{r}^2\exp(K)}\exp\left[-(1+K)\left(\frac{r}{\hat{r}}\right)^2 + \frac{2r}{\hat{r}}\sqrt{K(1+K)}\cos(\theta-\phi)\right]. \quad (7)$$

Following from this, and letting $K = 0$, we recover the Rayleigh joint envelope-phase PDF [16, eq. 2.201].

V. Phase PDF

Now integrating the joint envelope-phase distribution given in (5) with respect to the envelope, the phase PDF is obtained.

Theorem 3. *For $K, m \in \mathbb{R}^+, \phi, \theta \in [-\pi, \pi)$ the phase PDF is given by (8), where ${}_2F_1(\cdot,\cdot;\cdot;\cdot)$ is the Gaussian hypergeometric function.*

Proof: See Appendix C. ■

Some plots of the phase PDF given in (8) are shown in Fig. 2, alongside the results of Monte Carlo simulations. From Fig. 2 we observe that, as *m* decreases (i.e., as shadowing becomes more severe), the phase becomes progressively more dispersed, approaching a uniform distribution in the limit (as $m \to 0$), consistent with the phase distribution of Rayleigh-faded (non-LOS) signals. On the contrary, as *m* increases (i.e., the LOS fluctuations become smaller), the phase is more concentrated around its mean and its distribution approaches that of a Rician-faded signal without LOS shadowing. Although not shown here to maintain clarity, as $m \to \infty$ and $K \to 0$ the phase PDF degenerates to the uniform case. From Fig. 2, it is evident that the phase distribution is unimodal, reaching a maximum when $\theta = \phi$ and minimum when $\theta = \pi + \phi$, which is in stark contrast with the bimodal phase distribution of Hoyt-faded signals [17]. This demonstrates that the known relationship between Rician fading with LOS shadowing and Hoyt fading [18] does not hold for the phase.

VI. Performance Analysis

It is recalled here that the phase distribution is a fundamental statistic used to determine the average bit error probability ($\overline{P_{BE}}$) and the average symbol error probability ($\overline{P_{SE}}$) in phase-based modulation schemes [5]. For example, considering binary phase-shift keying (BPSK) the $\overline{P_{BE}}$ can be obtained as

$$\overline{P_{BE}^{BPSK}} = 2\int_{\pi/2}^{\pi} f_\Theta(\theta)\; d\theta; \quad (9)$$

further details of the equivalent calculations for quadrature phase-shift keying (QPSK) and 8-PSK can be found in [5].

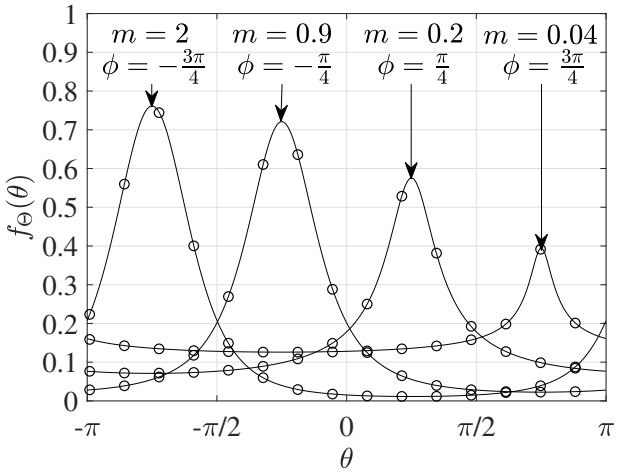

Fig. 2. Phase PDF given in (8) (solid lines) alongside Monte Carlo simulation (circles) for $K = 2$, with ϕ and m varying.

The $\overline{P_{SE}}$ for different M-ary PSK modulation schemes can be found through the evaluation of the following definite integral [5]

$$\overline{P_{SE}} = 2\int_{\pi/M}^{\pi} f_\Theta(\theta)\; d\theta, \quad (10)$$

where M is the modulation order. It is clear from (9) and (10) that when BPSK modulation is used, $\overline{P_{BE}} = \overline{P_{SE}}$. Typically, (9) and (10) are evaluated numerically due to the complexity of the integrations involved. However, using the derived result for the phase PDF, for the case when $\phi = 0$, a simple closed-form expression for the $\overline{P_{BE}}$ (or equivalently $\overline{P_{SE}}$) when using BPSK modulation can be found as follows.

Corollary 1. *For $K, m \in \mathbb{R}^+, \phi = 0$ when using BPSK modulation the $\overline{P_{BE}}$ can be obtained as*

$$\overline{P_{BE}^{BPSK}} = \frac{1}{2} - \frac{m^m\sqrt{K}\Gamma\left(m+\frac{1}{2}\right)}{\sqrt{\pi}\Gamma(m)(K+m)^{m+1/2}} \times {}_2F_1\left(m+\frac{1}{2},1;\frac{3}{2};\frac{K}{K+m}\right). \quad (11)$$

Proof: The proof is provided in Appendix D. ■

The $\overline{P_{BE}}$ for different M-ary PSK modulation schemes obtained using (9) is shown in Fig. 3. As we can see, the closed-form expression given in (11) matches exactly with the plots obtained through numerical evaluation and simulation for BPSK (i.e. $M = 2$) modulation. We observe that with a stronger LOS component (e.g. $K = 6$), the shadowing severity, m, has an appreciable impact on the $\overline{P_{BE}}$. We also see that, by increasing the modulation order, M, the impact of the LOS shadowing is reduced, albeit with the consequence of an overall higher $\overline{P_{BE}}$. With a weak LOS component (e.g $K = 0.25$), it is clear that m has a reduced effect on the $\overline{P_{BE}}$ and as $K \to 0$ it approaches the uniform case (i.e. Rayleigh).

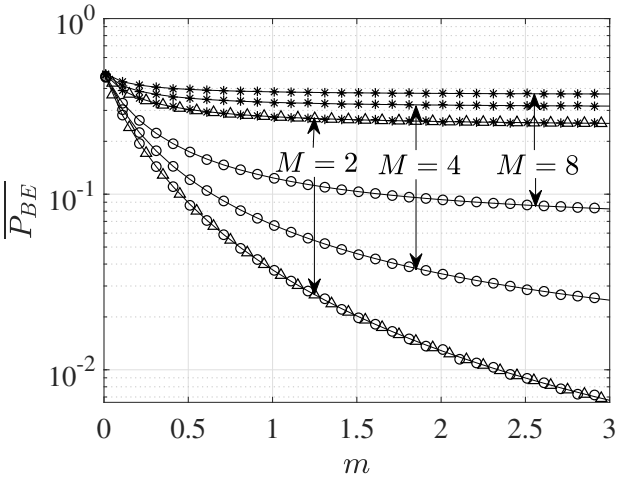

Fig. 3. $\overline{P_{BE}}$ evaluated using (9) (solid lines) alongside the closed-form expression for the BPSK (11) (triangles) and Monte Carlo simulation for $K = 0.25$ (asterisks) and $K = 6$ (circles), $\phi = 0$ with m varying, for BPSK, QPSK and 8-PSK modulation schemes.

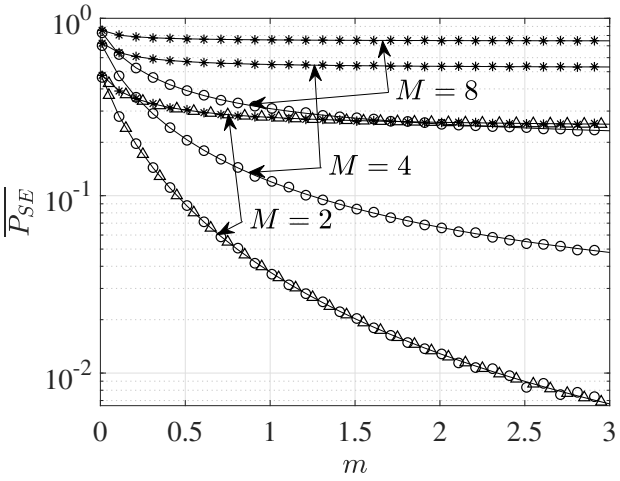

Fig. 4. $\overline{P_{SE}}$ evaluated using (10) (solid lines) alongside the closed-form expression for the BPSK (11) (triangles) and Monte Carlo simulation for $K = 0.25$ (asterisks) and $K = 6$ (circles), $\phi = 0$ with m varying, for BPSK, QPSK and 8-PSK modulation schemes.

In Fig. 4, it can be seen that when the shadowing severity is increased (i.e. lower values of m), the $\overline{P_{SE}}$ becomes elevated even for fading channels with a strong LOS (i.e. $K = 6$). This is particularly evident from Fig. 4 for the case when $K = 6$ and there is severe LOS shadowing ($m < 0.5$). In this instance, there is a significant rise in the $\overline{P_{SE}}$ achieved for all three of the modulation orders considered. This clearly demonstrates the importance of accounting for LOS shadowing in systems where this phenomena is likely to be encountered in order to achieve an accurate prediction of communications performance.

VII. Conclusion

The complex signal envelope of Rician fading, subject to LOS shadowing was presented and closed-form expressions for the quadrature, joint envelope-phase and phase distributions were derived. It was found that the shadowing of the LOS component has a remarkable impact on the phase, which is significantly more spread (or concentrated) around its mean as the shadowing is more (or less) pronounced. It was demonstrated that the relationship connecting the envelopes of Rician fading which undergoes LOS shadowing and Hoyt fading does not hold for the phase.

It is worth remarking that our new results will find use in the characterization of phase-based modulation techniques and in the performance analysis of wireless communication systems. To this end, we have provided two example applications, which evaluated the average bit error probability and average symbol error probability under different phase modulation schemes. For both applications, shadowing of the LOS signal was shown to have a noticeable impact. This was most predominant in situations where a strong LOS component exists which is subject to fluctuations caused by shadowing. Notably, despite the presence of a strong dominant component, increasing perturbation of the LOS signal can lead to significantly degraded performance irrespective of the phase modulation scheme used. Based on this observation alone, the importance of including LOS shadowing effects into the design of wireless systems which are likely to be susceptible to this physical propagation phenomena (such as those listed in [1]-[3]) cannot be overlooked.

Appendix A

The PDF of Z is obtained by unconditioning (3) with respect to ξ, whose PDF is given by

$$f_\xi(\xi) = 2\frac{m^m}{\Gamma(m)}\xi^{2m-1}\exp\big(-m\xi^2\big), \tag{12}$$

resulting in

$$\begin{aligned} f_Z(z) = {} & \frac{2m^m\sqrt{1+K}}{\sqrt{\pi}\;\hat{r}\;\Gamma(m)}\exp\left(-\frac{z^2(1+K)}{\hat{r}^2}\right) \\ & \times\int_0^\infty \xi^{2m-1}\exp\left[-\left(\frac{\lambda^2(1+K)}{\hat{r}^2}+m\right)\xi^2\right. \\ & \left.+\frac{\xi\lambda z2(1+K)}{\hat{r}^2}\right]d\xi. \end{aligned} \tag{13}$$

Following a sequential application of the identities in [19, eq. 3.462.1] and [19, eq. 9.240], (13) can be obtained in closed-form as given in (4).

Appendix B

From the model definition in (1), it can be seen that, when conditioned on ξ, X and Y are independent Gaussian random variables, with PDF given in (3). Following from this, their joint conditional PDF $f_{X,Y|\xi}(x,y;\xi)$ can be written as, $f_{X,Y|\xi}(x,y;\xi) = f_{X|\xi}(x;\xi)\times f_{Y|\xi}(y;\xi)$. Now using a Jacobian transformation, the conditional joint envelope-phase distribution is found as, $f_{R,\Theta|\xi}(r,\theta;\xi) = |J| f_{X,Y|\xi}(x,y;\xi)$, where $|J| = r$ is the Jacobian of the transformation. Expressing x and y in terms of r and θ, averaging over ξ, with PDF in (12), and sequentially applying the identities [19, eq. 3.462.1] and [19, eq. 9.240], in a similar manner to that used in Appendix A, the joint envelope-phase PDF (5) is found.

APPENDIX C

By integrating (5) with respect to R the phase PDF is found. This is achieved by splitting (5) into two separate integrals, which we denote here as *A* and *B*,

$$A = \frac{m^m(1+K)}{\pi\hat{r}^2(K+m)^m}\int_0^\infty r\exp\left(-\frac{r^2(1+K)}{\hat{r}^2}\right) \times {}_1F_1\left(m;\frac{1}{2};\frac{r^2(1+K)}{\hat{r}^2}\Delta(\theta,\phi)\right)dr, \tag{14}$$

$$B = \frac{2m^m(1+K)^{3/2}\Gamma(m+\frac{1}{2})\sqrt{K}}{\pi\hat{r}^3\Gamma(m)(K+m)^{m+1/2}}\cos(\theta-\phi) \times \int_0^\infty r^2\exp\left(-\frac{r^2(1+K)}{\hat{r}^2}\right) \times {}_1F_1\left(m+\frac{1}{2};\frac{3}{2};\frac{r^2(1+K)}{\hat{r}^2}\Delta(\theta,\phi)\right)dr. \tag{15}$$

Both (14) and (15) can be solved by first applying a quadratic transformation ($t = r^2$) and using the identity [19, eq. 7.621.4],

$$A = \frac{m^m}{2\pi(K+m)^m}{}_2F_1\left(m,1;\frac{1}{2};\Delta(\theta,\phi)\right), \tag{16}$$

$$B = \frac{m^m\sqrt{K}\Gamma(m+\frac{1}{2})}{2\sqrt{\pi}\Gamma(m)(K+m)^{m+1/2}}\cos(\theta-\phi) \times {}_2F_1\left(m+\frac{1}{2},\frac{3}{2};\frac{3}{2};\Delta(\theta,\phi)\right). \tag{17}$$

The resultant Gaussian hypergeometric function, ${}_2F_1(\cdot,\cdot;\cdot;\cdot)$, within (17) can be further simplified using the relationship [19, eq. 9.121.1],

$${}_2F_1(a,b;b;z) = (1-z)^{-a}. \tag{18}$$

Adding *A* and *B* together, followed by some tedious mathematical manipulations yields the exact closed-form expression given in (8).

APPENDIX D

The $\overline{P_{BE}}$ can be obtained for BPSK when $\phi = 0$, by using (16) and (17) and replacing the Gaussian hypergeometric function with its series definition [19, eq. 9.14.1]

$${}_2F_1(a,b;c;z) = \sum_{n=0}^{\infty}\frac{(a)_n(b)_n}{(c)_n n!}(z)^n, \tag{19}$$

and substituting into (9) with (6),

$$A = \sum_{n=0}^{\infty}\frac{(m)_n(1)_n K^n m^m}{\left(\frac{1}{2}\right)_n n!\pi(K+m)^{m+n}}\int_{\frac{\pi}{2}}^{\pi}\cos^{2n}(\theta)d\theta, \tag{20}$$

$$B = \sum_{n=0}^{\infty}\frac{\left(m+\frac{1}{2}\right)_n\left(\frac{3}{2}\right)_n K^n m^m\sqrt{K}\Gamma\left(m+\frac{1}{2}\right)}{\left(\frac{3}{2}\right)_n n!\sqrt{\pi}\Gamma(m)(K+m)^{m+n+1/2}} \times \int_{\frac{\pi}{2}}^{\pi}\cos^{2n+1}(\theta)d\theta. \tag{21}$$

Firstly, (20) is found by using [19, eq. 3.621.3], knowing $(2n)!! = 2^n(1)_n$, $(2n-1)!! = 2^n\left(\frac{1}{2}\right)_n$ and (18). Secondly, (21) is obtained using [19, eq. 3.621.4] with further mathematical manipulations and (19),

$$A = \frac{1}{2}, \tag{22}$$

$$B = -\frac{m^m\sqrt{K}\Gamma\left(m+\frac{1}{2}\right)}{\sqrt{\pi}\Gamma(m)(K+m)^{m+1/2}} \times {}_2F_1\left(m+\frac{1}{2},1;\frac{3}{2};\frac{K}{K+m}\right). \tag{23}$$

Adding (22) and (23) forms the exact expression given in (11).

REFERENCES

[1] A. Abdi, W. C. Lau, M. S. Alouini, and M. Kaveh, "A new simple model for land mobile satellite channels: first- and second-order statistics," *IEEE Trans. Wireless Commun.*, vol. 2, no. 3, pp. 519–528, May 2003.

[2] F. Ruiz-Vega, M. C. Clemente, J. F. Paris, and P. Otero, "Rician shadowed statistical characterization of shallow water acoustic channels for wireless communications," in *Proc. UComms Conf.*, Sestri, Italy, Sep. 2012, pp. 1–3.

[3] S. L. Cotton, "Human body shadowing in cellular device-to-device communications: channel modeling using the shadowed κ-μ fading model," *IEEE J. Sel. Areas Commun.*, vol. 33, no. 1, pp. 111–119, Jan. 2015.

[4] J. F. Paris, "Closed-form expressions for Rician shadowed cumulative distribution function," *Electron. Lett.*, vol. 46, no. 13, pp. 952–953, Jun. 2010.

[5] J. G. Proakis, "Probabilities of error for adaptive reception of M-phase signals," *IEEE Trans. Commun. Technol.*, vol. 16, no. 1, pp. 71–81, Feb. 1968.

[6] D. Hess, "Cycle slipping in a first-order phase-locked loop," *IEEE Trans. Commun. Technol.*, vol. 16, no. 2, pp. 255–260, Apr. 1968.

[7] J. G. Proakis and M. Salehi, *Digital Communications*, 5th ed. New York: McGraw-Hill, 2007.

[8] S. O. Rice, *Statistical Properties of Random Noise Currents*, N. Wax, Ed. New York: Dover, 1954, pp. 184–246.

[9] M. D. Yacoub, "Nakagami-m phase-envelope joint distribution: A new model," *IEEE Trans. Veh. Technol.*, vol. 59, no. 3, pp. 1552–1557, Mar. 2010.

[10] D. B. d. Costa and M. D. Yacoub, "The η-μ joint phase-envelope distribution," *IEEE Antennas and Wireless Propag. Lett.*, vol. 6, pp. 195–198, 2007.

[11] U. S. Dias and M. D. Yacoub, "The κ-μ phase-envelope joint distribution," *IEEE Trans. Commun.*, vol. 58, no. 1, pp. 40–45, Jan. 2010.

[12] J. F. Paris, "Statistical characterization of κ-μ shadowed fading," *IEEE Trans. Veh. Technol.*, vol. 63, no. 2, pp. 518–526, Feb. 2014.

[13] Abramowitz, M. and Stegun, I. A., *Handbook of Mathematical Functions*. US Dept. of Commerce, National Bureau of Standards, Applied Mathematics Series, 1972.

[14] G. Fraidenraich, J. C. S. S. Filho, and M. D. Yacoub, "Second-order statistics of maximal-ratio and equal-gain combining in Hoyt fading," *IEEE Commun. Lett.*, vol. 9, no. 1, pp. 19–21, Jan. 2005.

[15] Wolfram Research, Inc. The mathematical functions site. "Accessed on 03/20/2019". [Online]. Available: http://functions.wolfram.com/07.20.03.0001.01

[16] P. M. Shankar, *Fading and Shadowing in Wireless Systems*, 2nd ed. New York, USA: Springer International Publishing, 2017.

[17] R. S. Hoyt, "Probability functions for the modulus and angle of the normal complex variate," *Bell Sys. Tech. J.*, vol. 26, no. 2, pp. 318–359, Apr. 1947.

[18] L. Moreno-Pozas, F. J. Lopez-Martinez, J. F. Paris, and E. Martos-Naya, "The κ-μ shadowed fading model: unifying the κ-μ and η-μ distributions," *IEEE Trans. Veh. Technol.*, vol. 65, no. 12, pp. 9630–9641, Dec. 2016.

[19] I. S. Gradshteyn and I. M. Ryzhik, *Table of Integrals, Series, and Products*, 7th ed. San Diego, CA, USA: Academic Press, 2007.